The influence of microstructure on the sintering process in crystalline metal powders investigated by positron lifetime spectroscopy: III. Nickel reduction powder

1999 J. Phys.: Condens. Matter 11 1807

(http://iopscience.iop.org/0953-8984/11/7/011)

J. Phys.: Condens. Matter **11** (1999) 1807–1822. Printed in the UK PII: S0953-8984(99)80633-X

The influence of microstructure on the sintering process in crystalline metal powders investigated by positron lifetime spectroscopy: III. Nickel reduction powder

T E M Staab†§, R Krause-Rehberg†, B Vetter‡ and B Kieback‡

† Martin-Luther Universität Halle-Wittenberg, Fachbereich Physik, Friedemann-Bach-Platz 6, D-06108 Halle/Saale, Germany

‡ Technische Universität Dresden, Institut für Werkstoffwissenschaften, Momsenstraße 13, D-01062 Dresden, Germany

Received 3 January 1997, in final form 4 November 1998

Abstract. The sintering process in compacts of nickel reduction powder is investigated by positron lifetime spectroscopy. Additionally, the lifetime data obtained are compared to the data on the recovery and recrystallization after plastic deformation caused by cold rolling or pressing, and on the annealing out of vacancy clusters caused by low-temperature electron irradiation. Due to the small grain sizes inside the powder particles at lower temperature, positrons annihilate at grain boundaries, leading to vacancy-cluster-like signals. At intermediate temperature, a surface signal is detected (400–900 °C). This is in agreement with an effective powder-particle size of 3–5 μm estimated from scanning electron microscopy. When sintering starts, i.e. above 900 °C, the only detected defect signal, besides a small surface signal, stems from large-angle grain boundaries. At the intensive-shrinkage stage, there are contributions from different shrinkage mechanisms. The experimentally observed shrinkage rates can be explained by *Coble* creep which seems to dominate the material transport. *Nabarro–Herring* and *dislocation* creep play only minor roles in this system.

1. Introduction

Nickel is used technically in many important alloys and has often served as a model substance for fcc metals. Hence, accurate data on the activation energies for diffusion, and the annealing stages after deformation and irradiation are available, and studies of the sintering process using positron annihilation have been carried out previously [1, 2]. Since the theoretical foundations for describing the sintering process in compacts of metal powder used in technical applications—especially the shrinkage rate—are still controversial, we try to detect defects on an atomic scale by means of positron lifetime spectroscopy (POLIS). This gives us information about the parameters influencing the sintering process. So, we try to find indications of whether defect-induced diffusion or simple volume diffusion are possible mechanisms affecting this process.

Even though positron lifetime spectroscopy can be used to detect different lattice defects separately, some defects give the same signal, i.e. monovacancies, dislocations, and small-angle grain boundaries lead in nickel to a positron lifetime of about 160 ps while positron trapping at large-angle grain boundaries leads to a positron lifetime of about 300 ps, which is typical for vacancy clusters (agglomerations of 9–10 vacancies) [3]. The lifetimes of positrons trapped in

§ Present address: Helsinki University of Technology, Laboratory of Physics, PO Box 1100, FIN-02015 HUT, Finland.

0953-8984/99/071807+16$19.50

the image potential at metallic surfaces are about 450–650 ps [4–6]. Hence, it is important to determine powder-particle sizes and grain sizes inside powder particles. Then one can judge by using the results of the Monte Carlo (MC) simulation of the positron diffusion [7] and complementary investigations† which kind of defect may be detected at certain temperatures. It is important to know whether the defects are evenly distributed—allowing the application of the standard trapping model—or whether they are inhomogeneously distributed—e.g. with a defect-free interior of the grains with the positrons trapped exclusively at the boundaries (see the discussion in [8] and part I [9]).

In part I [9] we investigated the sintering of compacts of copper powders as an example representing fcc metals, and we considered compacts of tungsten powders as an example representing bcc metals in part II [10]; in the latter case, special attention was paid to the effect of different powder-particle sizes, which lead to different driving forces for sintering. In part III we investigate, finally, compacts of nickel reduction powder as another model substance for fcc metals.

'Sintering' means heating a compact up to approximately $4/5$ of its melting temperature in degrees Kelvin. The observed shrinkage is a pressureless process caused by the difference in free energy between the initial and final state. The energy difference is realized in one-phase systems by reducing all internal and external surfaces, i.e. pore walls and grain boundaries. The shrinkage rate depends on the morphology and microstructure of the powder and on process parameters such as the green density, heating rate, and sintering temperature. By *morphology* we mean the powder-particle size and shape, while *microstructure* includes the grain and subgrain sizes, dislocation density, etc.

It is commonly accepted that the material transport, which is necessary for the observed macroscopic shrinkage, is realized by a vacancy mechanism. What is questionable is what the relevant and active sources and sinks are: large- and small-angle grain boundaries (Nabarro–Herring creep), dislocations (Kosevic creep), or dissolving vacancy clusters; or alternatively the transport could be realized via grain boundary diffusion (Coble creep) or by dislocations via pipe diffusion. Part I [9] contains a brief discussion of the equations describing the above-mentioned mechanisms (for a comprehensive discussion, see [11] or [12]).

It is important to notice that the prevailing part of the shrinkage is obtained usually during the heating of the sample, i.e. when recrystallization is complete and grain growth is starting at higher temperatures.

Nabarro–Herring and Coble creep seem to be inappropriate for describing the observed high shrinkage rates if one takes the macroscopic particle size (e.g. that determined by screening) as a parameter‡, and if one neglects the inner structure of the powder particles§. But by considering an effective powder-particle size, one obtains shrinkage rates of the same order of magnitude as the observed ones [9, 10, 13].

We use as the positron source ^{22}Na, where the radioactive salt is placed between two thin (2 μm) Al foils. The measurement of the spectra is performed using a source–sample arrangement, where the source is placed between two identical samples (in a sandwich). As possible positron traps in metals (one-phase systems), we have: dislocations, monovacancies, vacancy clusters, interfaces (small- and large-angle grain boundaries), and internal surfaces (voids) (see the discussion in [8, 9]). For the detectable defect densities, nearly the same limits are valid as for copper (see [8]). In [8], the decomposition of multi-component spectra and the influences of a fine-grained structure or fine powder are discussed as well.

† We annealed out the radiation-induced defects, i.e. vacancies and (during annealing) vacancy clusters, and annealed out the defects created by plastic deformation.

‡ The effective powder-particle size after pressing is probably much smaller—by about one order of magnitude—due to the influence of powder agglomeration.

§ Neglecting the inner structure means more or less assuming the powder particles to be single crystals.

The outline of this article is as follows. In section 2, we describe the experimental set-up and the treatment of the samples. The results of our measurements are given in section 3, and will be discussed in section 4. Finally, section 5 contains our conclusions.

2. Experiments

In this section we explain the special features of the powders used for sintering, the experimental set-up for the dilatometer and positron lifetime measurements, and how we prepared the samples for and during the different measurements.

2.1. Nickel reduction powder

The nickel powder ('Puratronic') of 99.999% purity was supplied by Johnson–Matthey, Karlsruhe, Germany. The shape of the powder particles is irregular, but on average spherical. The powder particles themselves possess a complicated microstructure (dislocations, grain sizes) related to the production process, i.e. the temperature at which the reduction is performed. See table 1 for the particle size distribution for nickel reduction powder.

The morphology of the nickel reduction powder used here differs significantly from that of the nickel powder used in previous investigations, where the powder had a more sponge-like shape [1, 2, 14].

Table 1. The particle size distribution for nickel reduction powder. The analysis was performed using a laser granulator, 'Analysette 22' (Company: Fritsch GmbH, Idar-Oberstein). Please note that the SEM pictures indicate a much smaller effective powder-particle size. The powder tends to form large agglomerations.

Powder	d10 (μm)	d50 (μm)	d90 (μm)
Nickel reduction	9.2	24.7	59.4

2.2. Compaction, sintering, and positron lifetimes

The samples were pressed with a uniaxial pressure of 500 MPa. After pressing, the samples were sintered at the TU Dresden, where the shrinkage curves were measured *in situ* by a high-temperature dilatometer, i.e. we were continuously monitoring the shrinkage (corrected for thermal expansion). A reducing hydrogen atmosphere (heating rate: 50 K min^{-1}) and argon (heating rate: 10 K min^{-1}) were used. Expressing the sintering temperature of 1200 °C as a homologous temperature gives $T_S = 0.85\,T_M$, where T_M is the melting temperature of nickel in degrees Kelvin. For the POLIS measurement, small tablets were sintered in the furnace up to the appropriate temperature. Then they were cooled to room temperature by quickly removing them from the furnace, and hence 'freezing' a certain stage of the sintering process (see the discussion in [8]). Two identical samples (discs of diameter 11.5 mm and with a thickness of approximately 1 mm) were prepared for each temperature considered. For the measurements on the uncompacted powder, it was poured into a small box. Then the positron source was placed on the top, and powder again poured into the box. A standard fast–fast coincidence lifetime set-up with plastic scintillators was used (see [8] for details). As positron sources, we used ^{22}Na.

2.3. Electron irradiation and plastic deformation

Sintered samples (1200 °C, 4 h) were subjected to low-temperature (4 K) electron irradiation as follows: first they were cold rolled to achieve an approximate thickness reduction $\Delta d/d_0$

between 0.5 and 0.7, and then they were annealed at 1050 °C for 2 h, prior to irradiation. This ensures that the samples are free of defects that affect positrons (POLIS measurements gave a single-lifetime spectrum with $\tau_b = 103$ ps). Then these samples were irradiated with 2 MeV electrons, with a dose of 5×10^{18} cm^{-2} at 4 K, at the KFA Jülich. The source–sample sandwich was prepared after irradiation in liquid nitrogen, and put into the cryostat at 90 K. Hence, the vacancy-type irradiation defects cannot anneal out. The samples were then tempered in 20 K steps up to 440 K in the cryostat (measurement temperature: 90 K). After each temperature point had been reached, a positron lifetime spectrum was taken. Then the samples had to be transferred to another lifetime spectrometer for tempering at higher temperatures (measurement temperature: room temperature).

For the deformation experiment, the sintered samples (1200 °C, 4 h) were treated as follows: they were cold rolled to achieve an approximate thickness reduction $\Delta d/d_0 = 0.36$ (powder compacts). The same samples were then successively tempered under vacuum at each annealing temperature for 30 minutes, and, after that, cooled to room temperature again; this procedure was followed by the POLIS measurement.

To work out the influence of defects induced by pressing on the powder, we compacted the nickel powder. The following measurement included also the uncompacted powder with successively increasing pressure.

3. Results

In this section we present the results which will be discussed in section 4.

The powder-particle size estimated using a laser granulator seems to be too large, due to powder agglomeration, if one compares it to the size apparent from SEM pictures (see figure 1). Hence, we estimated an effective powder-particle size of 3–4 μm.

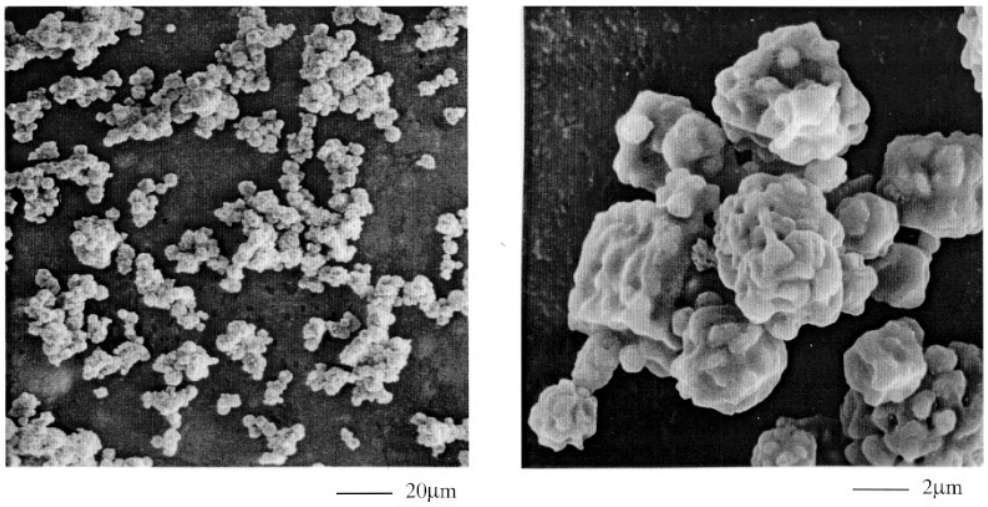

Figure 1. SEM pictures showing nickel reduction powder; the pictures indicate an effective powder-particle size of $\bar{L}_P = 3$–5 μm. Note the agglomerations leading to an average powder-particle size determined to be 24 μm.

3.1. Positron annihilation

Table 2 summarizes the data for positron lifetimes in the bulk and in defects, extracted from the literature [4, 5, 15–20].

Table 2. Positron lifetime data for nickel according to the cited literature in comparison to our work. The lifetimes for vacancies (τ_v) were determined in thermal equilibrium at 1500 K, '(thermal)', and after irradiation at 90 K, '(irradiated)'. The positron lifetime in vacancy clusters (τ_{cl}) depends on their size, while the surface lifetime (τ_{surf}) is generic. μ_v and μ_{disl} are the trapping coefficients for vacancies and dislocations.

	Schaefer [15]	Dlubek *et al* [16, 17]	Saoucha *et al* [18]	This work	Theory
τ_b (ps)	94	110	101 ± 2	102 ± 2	100 [19]
τ_v (ps) (thermal)	142	—	—	—	180 [20]
τ_v (ps) (irradiated)	—	—	—	168 ± 2	180 [20]
τ_{disl} (ps) (cold rolled)	—	150	—	157 ± 2	—
τ_{cl} (ps) (cluster)	—	200–450	—	220–350	200–450 [20]
τ_{surf} (ps) (surface)	—	—	—	500–600	450–600 [4, 5]
μ_v (10^{14} s^{-1})	1.5	—	—	—	—
μ_{disl} (cm^{-2})	—	1.1 ± 0.2	—	—	—

As we can see, the bulk lifetimes given, especially, differ quite markedly. This could be due to different source corrections used by the authors [21].

For the positron diffusion coefficient in nickel, we assume, due to lack of reliable data, the same value as for copper, $D_+ = 1.6$ cm^2 s^{-1}. This is quite reasonable, since these metals have the same lattice and are very similar in density and electron structure. D_+ is needed in the estimation of the grain and powder-particle sizes (see the discussion in part I [9]).

3.1.1. Recovery after plastic deformation. For comparison and to work out which defects in pressed powder samples are caused by the production process and which stem from pressing, we compacted the powder with different pressures (see figure 2). We see that the dislocation density increases with increasing pressure; this should be due to dislocation multiplication and/or formation of small-angle grain boundaries caused by plastic deformation.

In parallel, the intensity corresponding to the positron lifetime detected at surfaces (550 ps) decreases, due to a reduction of the powder-particle surface area with increasing green density. Another effect could be a reduced diffusion length of the positrons, since they become trapped at dislocations. The slight decrease of the intensity I_3 could have the same cause if the corresponding lifetime reflects trapping at grain boundaries. The average lifetime decreases, even though we are generating dislocations by pressing. This is due to the fact that the other lifetime components, already detected before pressing, are longer than the lifetimes of the dislocations.

During plastic deformation, dislocation glide and dislocation intersection certainly occur, and, hence, monovacancies could be generated via jog dragging (see chapter 7.3 of [22]). The vacancies could form vacancy clusters, since monovacancies in nickel are known to become mobile at about room temperature, and the sample heats up to above room temperature during cold rolling or pressing. See figure 3 for the results obtained for sintered samples of nickel reduction powder that have been plastically deformed.

We deformed pure nickel (the results were provided by Somieski [23]) as well as sintered samples by cold rolling (see [8]). The dislocation densities given are calculated according to the trapping model (see [8]) using the trapping coefficients given in table 2. From the annealing

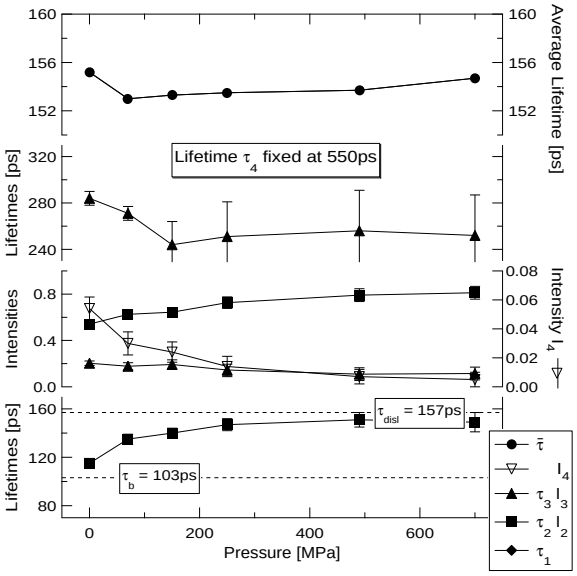

Figure 2. Successive compaction of as-produced nickel reduction powder ($\bar{L}_P = 24\ \mu$m), following uniaxial pressing. The lifetime for positrons trapped in surface states was fixed at 550 ps. This is necessary to stabilize the decomposition. The decrease of the average lifetime is due to generation of dislocations (the dislocation density includes small-angle grain boundaries).

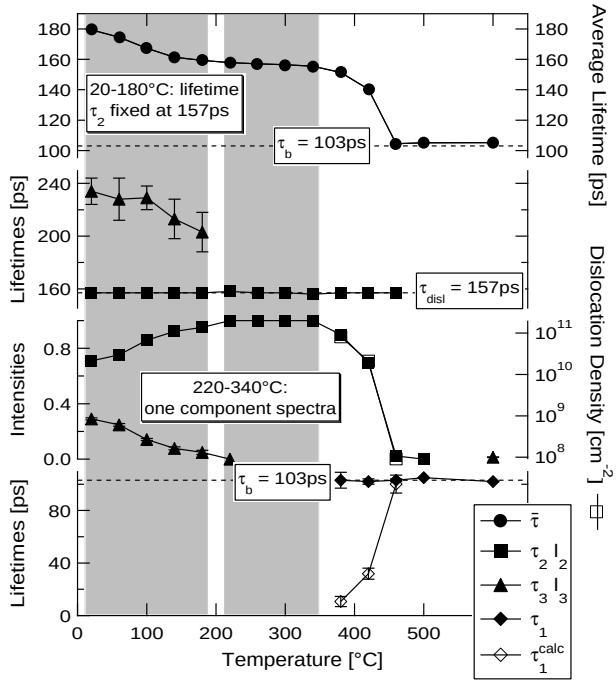

Figure 3. Pressed and sintered samples of nickel reduction powder (1200 °C for 4 h); after the pressing and sintering, they are cold rolled to achieve a thickness reduction of $\Delta d/d_0 = 0.36$ and annealed for 30 min at each temperature (6.0×10^6 counts per spectrum). The dislocation density drops from $>10^{11}$ cm^{-2} (20–340 °C) to below 3×10^8 cm^{-2} ($\geqslant$450 °C).

curve, we can see that vacancy clusters already present in the as-deformed state start to anneal out just above room temperature and vanish at about 220 °C, i.e. are no longer detectable using positrons—meaning that their intensity has dropped below 2×10^{-8} (see figure 3). The annealing stage between 100 and 200 °C has been observed previously by means of electrical resistivity measurement [24] and in positron studies on the annealing of the cold-worked state in pure nickel. The effect was seen in the average lifetime [17, 25] or in the peak-counting

rate [16]. Since no change in hardness is observed at that stage [25], it was attributed to the migration of point defects (non-equilibrium vacancies), because recrystallization of 90% of cold-rolled pure (5N8) nickel is observed at about 300 °C [17, 24], but a multi-component analysis of the positron lifetime data was not discussed. This annealing stage is observed after quenching by means of electrical resistivity as well. After annealing the samples at 200 °C, the authors of [26] find prismatic loops by means of TEM, and speculate on their formation by collapsing vacancy clusters.

Between 220 and 340 °C, we observe complete trapping of positrons into dislocations, meaning that the dislocation density is above 6×10^{10} cm^{-2}. Only the dislocation signal persists up to 500 °C, where the density drops below 2×10^{8} cm^{-2}, indicating that recrystallization is complete. The trapping model analysis indicates deviations for the temperature range in which recrystallization has its onset. This is apparently due to an inhomogeneous distribution of recrystallized grains (see the discussion in [8]).

3.1.2. Annealing out of quenched-in and irradiation-induced defects. We investigate the annealing out of defects—mainly monovacancies—after low-temperature electron irradiation. Even though this was studied extensively in the 1970s and early 1980s for copper (see part I and references given therein), not much work on nickel has been reported.

Furthermore, a multi-component decomposition was not performed at that time, and most of the earlier work report only Doppler-broadening data, from which the identification of different defects is difficult.

Previous studies on copper after irradiation with 2 MeV electrons at 4 K with a dose of 5×10^{22} m^{-2} detected only a vacancy signal (a single-lifetime spectrum) with a lifetime of about 170 ps, up to 220 K. Then, vacancy clustering is observed. The studies performed by us had the aim of obtaining accurate values for positron lifetimes in monovacancies and typical lifetimes in vacancy clusters, and, additionally, of studying their respective behaviours following annealing [3]. To work out whether impurities play a dominant role or not, we irradiated sintered samples as well.

After electron irradiation, pure nickel shows a single-lifetime spectrum, i.e. complete trapping in one defect type (as confirmed by MELT—see [8]), of lifetime 168 ± 0.5 ps [8], while the sintered sample, in the as-irradiated state, shows a two-component spectrum with a defect lifetime of 168 ± 1 ps (see figure 4). We can certainly attribute the lifetime of 168 ps to monovacancies, since dislocations are not likely to exist in the samples. The calculated lifetime of positrons in monovacancies is $\tau_v = 163$ ps [3], while older calculations obtained $\tau_v = 180$ ps [20]. These results are in sufficient agreement with the experimental value.

The decrease of the average lifetime and the defect intensity at about 270 K indicates the onset of vacancy migration. The changes in the defect-related positron lifetime at 320 K (for pure nickel—see [8]) and at 380 K (for sintered nickel), from 168 to 157 ps, could indicate that dislocation loops are formed, while no clustering is observed. Vacancy clustering is observed at slightly higher temperatures (470 K), where we see an increase in the average lifetime while the defect lifetime takes a value typical for vacancy clusters. Vacancy clustering in the temperature range 200–300 °C has been seen after cold rolling due to the influence of impurities [17], but this is questionable here, since we did not observe clustering in the annealing experiment performed, after cold rolling, on the same material as was used in the irradiation experiments (see section 3.1.1).

The deviations from the trapping model between 300 and 500 K could be caused by there being two lifetime components for vacancies and dislocations which cannot be resolved, and hence lead to a value of τ_1 that is too high (see the discussion in [27]).

Vacancy migration starts at about 0 °C, as is observed after quenching by means of

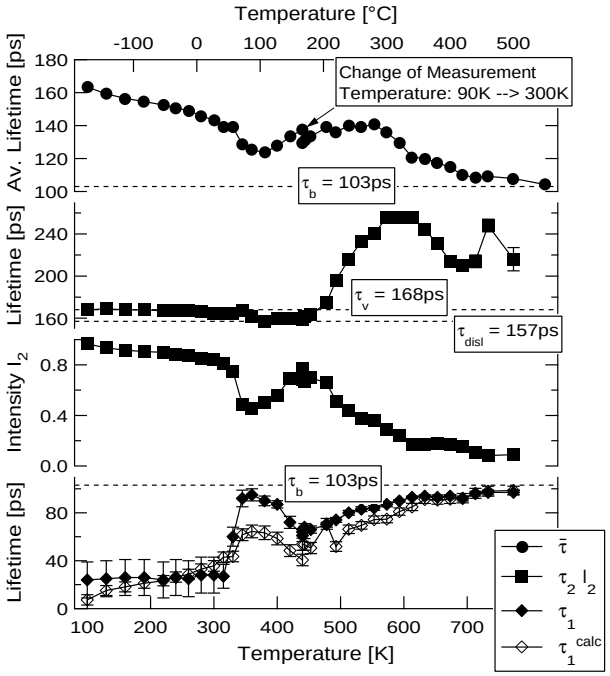

Figure 4. Recovery of electron-irradiated sintered nickel reduction powder samples. The samples were reduced in thickness by cold rolling (to about $\Delta d/d_0 = 0.5$), and then annealed at 1050 °C for 2 h prior to irradiation (measurements gave the bulk lifetime). The vacancy density in the as-irradiated state is slightly below 8×10^{-4}.

electrical resistometry [26, 28]. The authors of [26, 28] obtain a vacancy migration enthalpy of 1.2 ± 0.2 eV, a vacancy formation enthalpy of 1.8 ± 0.2 eV, and an entropy factor of $0.45\ k_B$. These values are in good agreement with Doppler-broadening data on vacancies in thermal equilibrium [29].

3.1.3. Annealing of uncompacted powder. To work out which of the defects detected in compacts are present in the as-produced state of the powder and which are generated by pressing, we carried out an annealing experiment on the uncompacted powder (see figure 5). The decomposition of the lifetime spectra reveals at least four different lifetimes, which can be attributed as reflecting positron trapping at surface states ($\tau_{surf} \approx 550$ ps), and at grain boundaries ($\tau_{GB} \approx 300$ ps), or can be described as $\tau_1 = 110$–120 ps.

Since the measured lifetime is slightly higher than we would expect from undisturbed parts of the crystal ($\tau_b \approx 103$ ps), we might suspect that the lifetime detected is a combination of τ_b with a dislocation lifetime. But the dislocation lifetime cannot be separated out, due to the very small corresponding intensity, i.e. low dislocation density.

From the lifetime data together with the results from the Monte Carlo simulation of the positron diffusion [7], we can estimate averages for powder-particle and grain sizes.

The results are given in table 3. So, under the assumption of nearly spherical shapes, the average powder-particle size can be estimated to be $\bar{L}_P = 4.1 \pm 1.0\ \mu$m, while we obtain for the average grain size with the sample in the as-produced state $\bar{L}_G = 1.7 \pm 0.3\ \mu$m.

3.1.4. Sintering. We can assume that positrons in powders or porous materials thermalize inside compact material and then start diffusing. Hence, they can reach interfaces and surfaces (see the discussion in part I and [8]).

If we detect a surface component, a significant part of the total signal stems from the contact

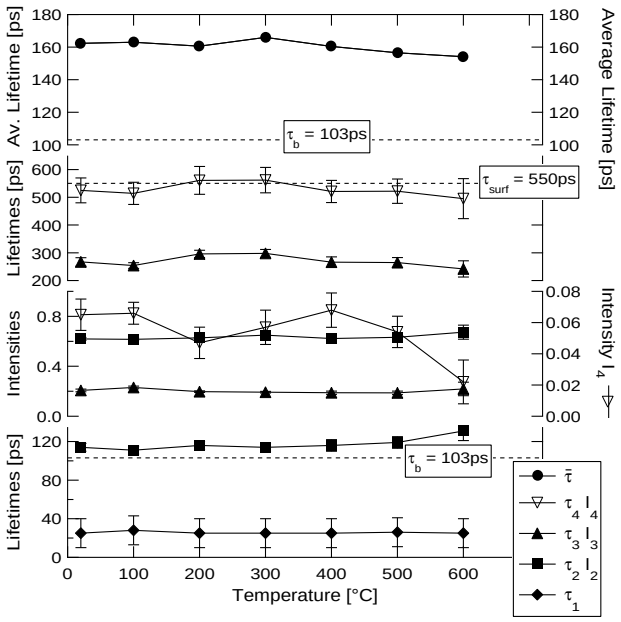

Figure 5. Uncompacted nickel reduction powder annealed at the given temperature for 30 min in a furnace under vacuum. The average lifetime decreases only slightly even though we have passed the recrystallization temperature ($T_R \approx 0.4\ T_M = 418\ ^\circ$C). Since we detect a bulk lifetime, large-angle grain boundaries ($\tau_{GB} \approx 300$ ps) and surface states ($\tau_{surf} \approx 550$ ps) are the most probable positron traps. The lifetime spectra were taken using 15×10^6 counts per spectrum.

Table 3. The fractions of positrons reaching the powder-particle surfaces (η_{surf}) and trapped at the grain boundaries (η_{GB}) estimated from lifetime analysis. The values for the powder-particle sizes ($\bar{L}_P$) and grain sizes ($\bar{L}_G$) are estimated with the help of the MC simulation of the positron diffusion.

T (°C)	η_{surf}	κ_{GB} (10^9 s^{-1})	$\bar{L}_P$ (μm)	η_{GB}	$\bar{L}_G$ (μm)
20	0.061	5.82	4.5 ± 2.0	0.18	1.7 ± 0.5
100	0.063	7.50	3.0 ± 1.5	0.21	1.3 ± 0.5
200	0.044	4.93	5.0 ± 2.0	0.17	1.8 ± 0.5
300	0.054	5.71	4.0 ± 2.0	0.17	1.8 ± 0.5
400	0.063	4.80	3.5 ± 2.0	0.16	1.9 ± 0.5
500	0.050	4.72	4.5 ± 2.0	0.16	1.9 ± 0.5
Average	—	—	4.1 ± 1.0	—	1.7 ± 0.3

boundaries or the contact boundary area (see figure 6, where we find a surface component in the decomposition of the lifetime spectra).

From the positron lifetime spectra, we find that there are at least three different types of defect present. As shown in figure 5, we find even for the uncompressed powder a signal which could be a combination of those from dislocations or small-angle grain boundaries with the bulk lifetime, a vacancy-cluster-like signal (lifetime $\approx$ 300 ps: vacancy clusters in the volume or large-angle grain boundaries), and a surface lifetime ($\approx$550 ps). We can assume that each surface state has a definite lifetime. This justifies the later fixing of the surface lifetime at 550 ps, which is necessary to stabilize the decomposition of the spectra.

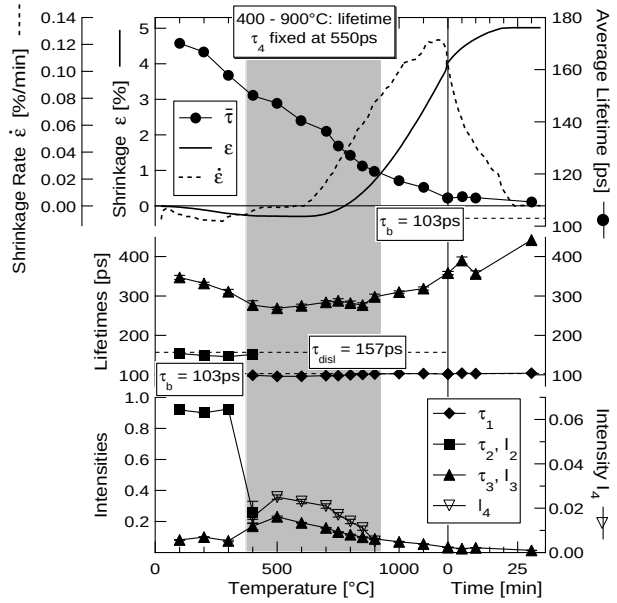

(a)

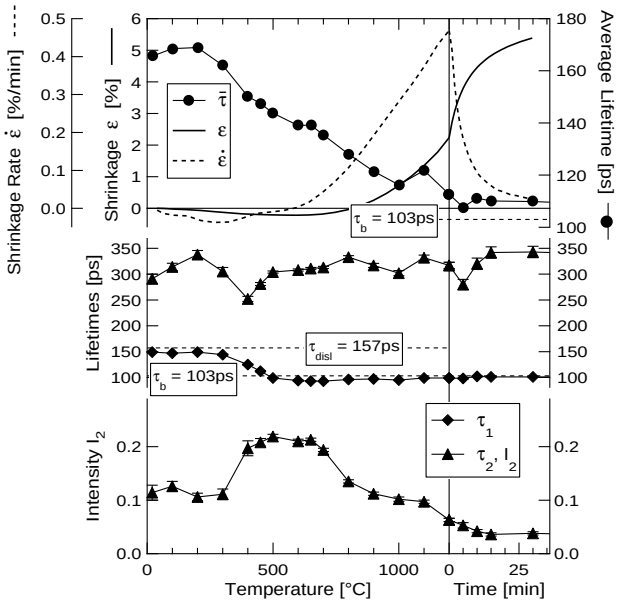

(b)

Figure 6. Compacts of nickel reduction powder ($\bar{L}_P = 24\ \mu$m), pressed to a green density $\rho_g = 0.78\ \rho_0$ and sintered at a heating rate of 10 K min^{-1} under Ar (6.0×10^6 counts per spectrum) (a) and at 50 K min^{-1} under H_2 (1.5×10^6 counts per spectrum) (b); the figures show the shrinkage and the shrinkage rate together with the average lifetime (upper part), and a decomposition of the lifetime spectra (lower part). We fixed an apparent surface lifetime at a plausible value of 550 ps (a). The dislocation density drops from $>10^{11}$ cm^{-2} to below 3×10^8 cm^{-2} between 300 and 500 °C.

From figure 6(a) we see that dislocations are annealing out at about 400 °C, indicating recrystallization. Due to the decreased defect density, the diffusion lengths of positrons increase and we observe from 400 °C onwards a surface component. Hence, some positrons reach the pores on their diffusion path. The increase in the intensity I_3 probably has the same cause, i.e. the diffusion to the boundaries is made easier for positrons. When the sintering process starts at about 700 °C, besides a surface lifetime with a very small intensity, only two components are found: $\tau_1 \approx \tau_b$ and $\tau_2 \approx \tau_{cl}$. The intensity I_2 slowly decreases with further increasing temperature while sintering is starting; i.e. the shrinkage rate rises from zero. The surface lifetime vanishes at 1000 °C, indicating a decreasing porosity.

For a heating rate of 50 K min^{-1} (figure 6(b)) we could not resolve more than two lifetime components due to poor statistics. Nevertheless, the main features are found here as well: dislocations annealing out above 400 °C, and $\tau_1 \approx \tau_b$ and $\tau_2 \approx \tau_{cl}$ when the sintering is starting.

4. Discussion

This section starts with a discussion of the experiments on the annealing out of defects after plastic deformation and electron irradiation. The results obtained help us to interpret the lifetime analysis of the sintered samples. See figure 7 for a comparison of the changes in the average lifetimes with temperature.

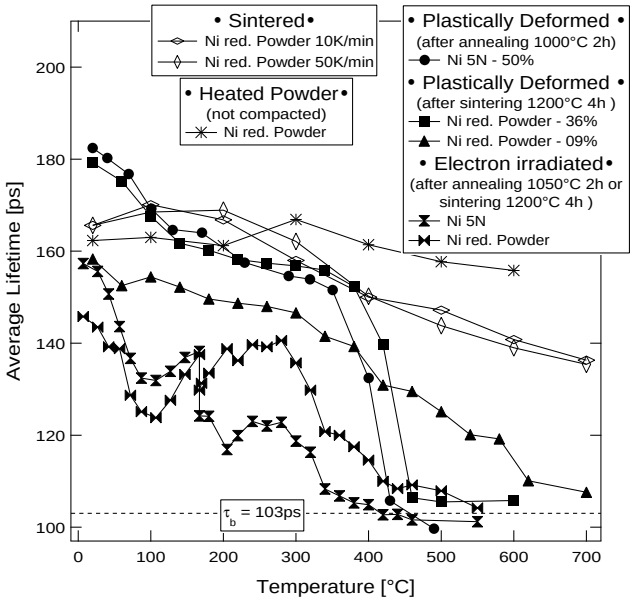

Figure 7. Annealing behaviour up to 700 °C for all of the differently treated samples. Note the similarity in annealing behaviour between uncompacted and compacted nickel powder. On the other hand, defects induced by electron irradiation and plastic deformation have annealed out at 600 °C.

4.1. Plastic deformation

Sintered compacts of nickel reduction powder (1200 °C, 4 h) were plastically deformed by cold rolling. Directly after the deformation, we observe from each sample material a vacancy-

cluster signal and a dislocation signal, while all positrons are trapped into defects at degrees of deformation higher than about $\Delta d/d = 0.3$. The vacancy-cluster signal vanishes at about 220 °C for the sample material, while the dislocation signal vanishes between 350 and 600 °C according to the degree of deformation (see figures 3 and 7 for the results for pure bulk nickel; see also [8]).

4.2. Electron-irradiated samples

Monovacancies generated by irradiation become mobile at about 270 K. This is reasonable, in view of an activation energy for vacancy migration of 1.04 ± 0.1 eV. In this temperature range, clustering is not observed, but the defect signal changes from a vacancy value to a dislocation value, meaning that vacancies would be directly converted into dislocation loops. During subsequent annealing above 500 K, the lifetime of the positrons in defects increases, which normally indicates vacancy clustering. But the vanishing of vacancy-cluster signals occurs at higher temperature than after plastic deformation, even though the same sample material was used as for figures 3 and 4 (for the results for pure nickel, see [8]).

4.3. Heated powder

Taking uncompacted powder in the as-produced state and heating it over the same temperature range as for the deformed and irradiated samples leads only to a very slight decrease in the average lifetime (see figures 5 and 7). Since dislocations and vacancy clusters should already have annealed out for $T > 400$ °C, only large-angle grain boundaries inside the powder particles and a small effective powder-particle size can explain the POLIS data. Apparently, no dislocations are present with sufficiently high densities in the as-produced state, since we did not detect a dislocation signal. Since the vacancy-cluster-like lifetime does not change its intensity, grain growth is expected above 600 °C. The positron lifetime detected, about 550 ps, which is typical for capture in surface states, indicates powder-particle sizes below 15 μm. Considering its corresponding intensity together with the Monte Carlo simulation results, we can estimate a powder-particle size of 4.1 ± 1.0 μm (see table 3), which is in agreement with SEM pictures giving 3–5 μm (see figure 1).

4.4. Sintered samples

As regards, the sintered samples, we can say that compacts of the nickel powder show a very complicated defect structure for temperature below 950 °C, where we detect three different positron lifetimes typical for defects, i.e. lifetimes for positrons trapped at dislocations, in vacancy clusters, and at surfaces (see figure 6). Dislocations are obviously annealing out between 300 and 500 °C, which is also the temperature range over which recrystallization after plastic deformation takes place. The cluster intensity increases, and a positron lifetime typical for trapping at surfaces (about 550 ps) becomes visible when the dislocations have annealed out† (see figure 6(a)). The detection of a positron lifetime at surfaces indicates a powder-particle size of less than 15 μm. The signal reflecting the vacancy-cluster-like lifetime—present even for uncompacted powder—increases in relative intensity during the annealing out of dislocations and then subsequently decreases with increasing temperature above 500 °C. Since we know from plastic deformation and electron irradiation results that the vacancy clusters that were in the volume have annealed out at that temperature, only large-angle grain boundaries can act as positron traps in that temperature region. This assertion is

† This is because the positron diffusion length has increased due to a lowering of the defect density inside the grains.

supported by the decomposition of the spectra; the fact that $\tau_1 \approx \tau_b$ indicates annihilation of the major part of the positrons in the defect-free interior of recrystallized grains (see figure 6 and the discussion in part I [9] and [8]).

We see for temperatures above 600 °C, as indicated by a positron lifetime of about 300 ps and its decreasing intensity, grain growth inside each powder particle. As the sintering temperature is approached, the contact boundaries start moving, causing the grain size to become larger than the original powder-particle size.

4.5. Possible sintering mechanisms

The contributions to the material transport arising from different sintering mechanisms have been extensively discussed in part I [9]. We will calculate the Nabarro–Herring creep, Coble creep, and dislocation creep according to the equations given in part I. The two-particle model uses equations given in part I as well. We estimate the shrinkage rates in figure 8 for diffusional creep according to the lifetime data, giving $\bar{L}_P$ and $\bar{L}_G$, while the two-particle model uses the experimentally determined shrinkage and $\bar{L}_P$. As we did to obtain the results given in table 3, we calculate from the lifetime data the fraction of positrons reaching surfaces and interfaces by using the trapping model. This, together with the Monte Carlo results on positron diffusion [7], gives the effective grain sizes $\bar{L}_G$ and powder-particle sizes $\bar{L}_P$. The powder-particle size used for the calculations is fixed at the average obtained from the powder measurement (see table 3), i.e. at $\bar{L}_P = 4.1\ \mu$m. The relevant constants for the calculation, given below, were taken from [30]: the Boltzmann constant $k_B = 8.617 \times 10^{-4}$ eV K^{-1}; the volume diffusion coefficient $D_{vol} = D_0^{vol} \exp(-Q_{vol}/k_B T)$ ($D_0^{vol} = 0.6 \times 10^{-4}$ m^2 s^{-1}, $Q_{vol} = 2.71$ eV); the grain boundary diffusion coefficient $D_{GB} = D_0^{GB} \exp(-Q_{GB}/k_B T)$ ($D_0^{GB} = 0.068 \times 10^{-4}$ m^2 s^{-1}, $Q_{GB} = 1.19$ eV); the surface tension $\gamma_S = 1.777$ J m^{-2}; the grain boundary tension $\gamma_{GB} = 0.866$ J m^{-2}; the atomic volume $\Omega = 1.09 \times 10^{-29}$ m^3; the effective cross section of grain boundary diffusion $\delta_{GB} = 5.12 \times 10^{-10}$ m; and the geometric constants $A_0 = 1$–4, $A_1 \approx 10$, $A_2 \approx 150$ from [11], while the porosity Θ is calculated from shrinkage data.

Using the results for the effective powder-particle size, Nabarro–Herring creep gives shrinkage rates that are one order of magnitude too small. A significant contribution is noticed only 100–200 °C below the sintering temperature. Coble creep gives approximately the right shrinkage rates. Dislocation creep is not considered, since the positron results indicate that the dislocation density is globally less than 2×10^8 cm^{-2} for temperatures above 600 °C (see figure 7). Hence the relation $N_{disl} > 1/(\delta \bar{L}_G^2)^{2/3}$ is not obeyed, meaning that dislocations, acting as vacancy sources and sinks, are not denser than grain boundaries for the given grain sizes [11]. We included in figure 8 the calculation of the Coble creep, with the sizes of the large-angle grain boundaries inside powder particles as parameters. As we can see, the estimated shrinkage rate becomes too high (400–800 °C). This shows that small grain sizes or movable dislocations can enhance the material transport only if their separation becomes smaller than double the curvature of the neck (the influence area of the Laplace tension). Because the models contain some approximations and the parameters are not known with sufficient accuracy, one cannot expect an exact coincidence.

Using instead the modified two-particle model, the shrinkage rates estimated are too high by a factor of 20–30. In order to present them in figure 8 together with the other model calculations, we scaled the results by the given factors. We did not find a quantitative coincidence, but the qualitative tendencies of the shrinkage rates described by this model and those determined experimentally are quite similar. Perhaps the rates are too high due to an underestimation of the influence of surface diffusion, which has been neglected. Surface diffusion leads to neck growth without shrinkage, and can change the curvature of the neck,

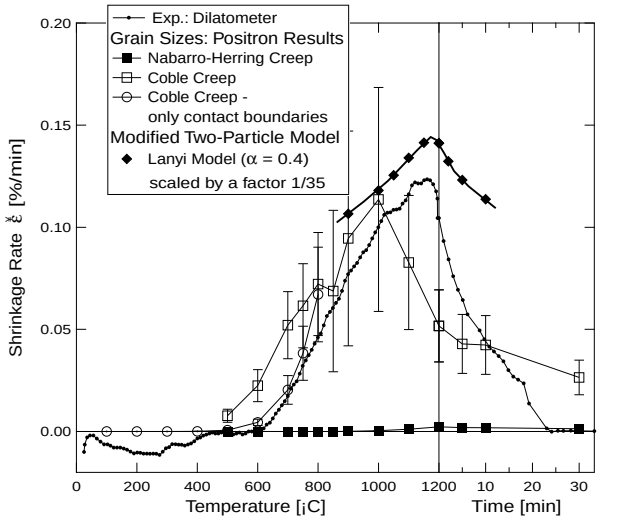

(a)

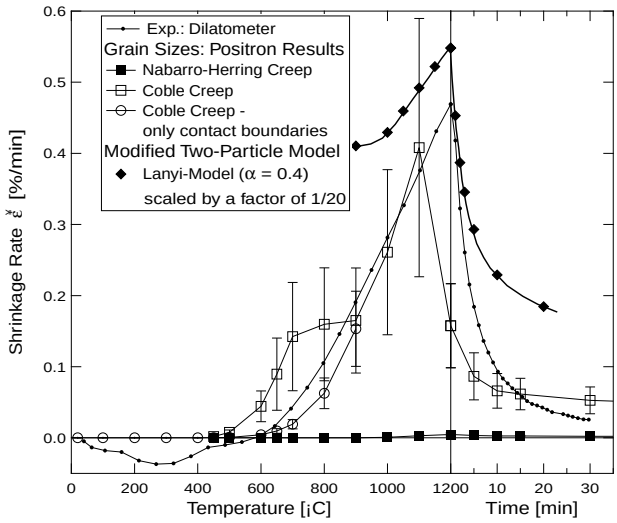

(b)

Figure 8. Shrinkage rates for different mechanisms as estimated from experimental results; compacts of nickel reduction powder were sintered at heating rates of 10 K min^{-1} (a) and 50 K min^{-1} (b). The decrease of the calculated shrinkage rate is due to grain growth; the grain size becomes significantly larger than the powder-particle size (Coble creep).

hence reducing the driving force for sintering. Another reason could be the deviation of the forms of the powder particles from the assumed spherical shape.

5. Conclusions

The effective powder-particle size revealed by SEM pictures is much smaller than that determined by particle-size analysis. Hence, the driving force for sintering is much larger, since it is proportional to the inverse particle size.

Vacancy clusters in the volume, as observed after electron irradiation and plastic deformation, anneal out before the cluster-like signal disappears for pressed and sintered samples. Hence, this cluster signal is interpreted as positron annihilation at grain boundaries. This interpretation is, for copper, in good agreement with grain sizes determined by metallography and estimated from a Monte Carlo simulation of the positron diffusion.

From positron lifetime spectroscopy (POLIS) data, we can conclude that the powder particles possess inner microstructure, i.e. there are large- and small-angle grain boundaries and/or dislocations, due to the production process. The greater part of positron trapping ($\tau \approx 300$ ps) must be due to grain boundaries, since uncompacted heated powders did not show any annealing stage up to 600 °C. Hence, vacancy clusters or dislocations do not seem to be responsible for the positron trapping, since the stages in which they anneal out have been observed to occur at about 200 °C and 400 °C, respectively (see also figure 7). During pressing, the dislocation density is increased in the powder compacts with increasing pressure. It is possible that vacancy clusters are also generated, but they are difficult to detect against the background of the other signals with a similar lifetime, apparently arising from grain boundaries.

Hence, we are, essentially, detecting, by means of POLIS, recovery and recrystallization. Above $T_R = 0.4\,T_M$, the decreasing intensity corresponding to the cluster-like lifetime of about 300 ps is due to grain growth. At the temperature where the sintering is starting, the POLIS data indicate a defect-free interior of the grains and positron trapping only at grain boundaries.

Hence, by modelling the diffusion to grain boundaries and surfaces on the basis of positron data, we have estimated an average grain size inside the powder particles which is used in the model calculations for the shrinkage rate. These calculations give, under the assumption of an effective powder-particle size, estimated from POLIS and SEM, reasonable shrinkage rates. We find that Coble creep (grain boundary diffusion) is in good agreement with the shrinkage rates obtained experimentally if we assume contact boundaries to be the only effective vacancy sinks. This is justified in view of the limited range of the Laplace tension.

Underestimation of the influence of surface diffusion could cause the shrinkage rates estimated on the basis of the modified two-particle model to be too high, because then the curvature gradients are reduced much more than is described by the model. Hence the driving force is lower than that assumed.

Acknowledgments

We would like to thank Professor W Schatt and Dr K-P Wieters (both at TU Dresden) for many interesting discussions, W Zeiger (TU Dresden) for the preparation of the sintered samples (part of his diploma thesis work), Dr F Dworschak (KFA Jülich) for preparing the electron-irradiated samples, F Rudolf (University Halle) for preparing the source–sample sandwich and performing the low-temperature lifetime measurements on the electron-irradiated samples, and B Somieski (Universität Halle-Wittenberg) for the results on deformed pure nickel.

References

[1] Schatt W and Hinz M 1988 On the generalizability of defect-activated sintering *Powder Metall. Int.* **20** 17–20

[2] Krause R, Schatt W, Vetter B and Polity A 1990 Study of sintering processes in copper and nickel by positron annihilation *Cryst. Res. Technol.* **25** 819–25

[3] Staab T E M, Petters K, Hübner C G and Polity A 1999 Multi-component positron lifetime analysis of the annealing behavior in electron-irradiated and plastically deformed high-purity metals, to be published

[4] Lynn K G, Frieze W E and Schultz P J 1984 Measurement of the positron surface-state lifetime for Al *Phys. Rev. Lett.* **52** 1137–40

[5] Nieminen R M, Puska M J and Manninen M 1984 Comment on the positron surface-state lifetime *Phys. Rev. Lett.* **53** 1298
[6] Steindl R, Kögel G, Sperr P, Willutzki P, Britton D T and Triftshäuser W 1992 Positron lifetimes on clean metallic surfaces *Mater. Sci. Forum* **105–110** 1455–8
[7] Hübner Ch, Staab T and Krause-Rehberg R 1995 Positron diffusion in fine-grained materials—a Monte Carlo simulation *Appl. Phys.* A **61** 203–6
[8] Staab T E M, Krause-Rehberg R and Kieback B 1999 Positron annihilation in fine-grained materials and fine powders—an application to sintering of technically used metal powders *J. Mater. Sci.* at press
[9] Staab T E M, Krause-Rehberg R, Vetter B and Kieback B 1999 The influence of microstructure on the sintering process in crystalline metal powders investigated by positron lifetime spectroscopy: I. Electrolytic and spherical copper powders *J. Phys.: Condens. Matter* **11** 1757
[10] Staab T E M, Krause-Rehberg R, Vetter B, Kieback B, Lange G and Klimanek P 1999 The influence of microstructure on the sintering process in crystalline metal powders investigated by positron lifetime spectroscopy: II. Tungsten powders with different powder-particle sizes *J. Phys.: Condens. Matter* **11** 1787
[11] Schatt W 1992 *Sintervorgänge* 1st edn (Düsseldorf: VDI)
[12] Geguzin Ja E 1973 *Physik des Sinterns* 1st edn (Leipzig: VEB Deutscher Verlag für Grundstoffindustrie)
[13] Hübner C G, Staab T and Leipner H S 1995 TEM studies of the microstructure of pressureless sintered copper *Phys. Status Solidi* a **150** 653–60
[14] Brand K 1993 Zum Einfluß der Interdiffusion auf die Verdichtung beim Festphasensintern von Zweikomponentensystemen mit vollständiger Löslichkeit der Komponenten *PhD Thesis* Technische Universität Dresden
[15] Schaefer H E 1987 Investigation of thermal equilibrium vacancies in metals by positron annihilation *Phys. Status Solidi* a **102** 47–65
[16] Dlubek G, Brümmer O, Meyendorf N, Hautojärvi P, Vehanen A and Yli-Kauppila J 1979 Impurity-induced vacancy clustering in cold-worked nickel *J. Phys. F: Met. Phys.* **9** 1961–73
[17] Dlubek G, Krause R, Brümmer O, Michno Z and Gorecki T 1987 Impurity-induced vacancy clustering in cold-rolled nickel alloys as studied by positron annihilation techniques *J. Phys. F: Met. Phys.* **17** 1333–47
[18] Saoucha A, Pedersen N J and Eldrup M 1992 On source contributions to positron lifetime spectra *Mater. Sci. Forum* **105–110** 1971–4
[19] Puska M J and Nieminen R M 1994 Theory of positrons in solids and on solid surfaces *Rev. Mod. Phys.* **66** 841–97
[20] Puska M J and Nieminen R M 1983 Defect spectroscopy with positrons: a general calculational method *J. Phys. F: Met. Phys.* **13** 333–46
[21] Staab T E M, Somieski B and Krause-Rehberg R 1996 The data treatment influence on the spectra decomposition in positron lifetime spectroscopy; part 2: The effect of source corrections *Nucl. Instrum. Methods* A **381** 141–41
[22] Hull D and Bacon D J 1984 *Introduction to Dislocations* 3rd edn (Oxford: Pergamon)
[23] Somieski B 1996 Positronenlebensdauerspektroskopie an mechanisch geschädigten Eisenlegierungen *PhD Thesis* Universität des Saarlandes und Martin-Luther Universität Halle-Wittenberg
[24] Seeger A 1955 Theorie der Gitterfehlstellen *Kristallphysik 1 (Handbuch der Physik vol 4)* ed S Flügge (Berlin: Springer) pp 383–667
[25] Byrne J G A 1979 Review of positron studies of the annealing of the cold worked state *Metall. Trans.* A **10** 791–807
[26] Wycisk W and Feller-Kniepmeier M 1976 Quenching experiments on high-purity nickel *Phys. Status Solidi* a **37** 183–91
[27] Somieski B, Staab T E M and Krause-Rehberg R 1996 The data treatment influence on the spectra decomposition in positron lifetime spectroscopy; part 1: On the interpretation of multi-component analysis studied by Monte Carlo simulated model spectra *Nucl. Instrum. Methods* A **381** 128–40
[28] Troev T, Angelov Ch and Mincov I 1989 Positron annihilation measurement of quenched-in defects in Ni *Phys. Lett.* A **138** 65–8
[29] Smedskjaer L C, Fluss M J, Legnini D G, Chason M K and Siegel R W 1981 The vacancy formation enthalpy in Ni determined by positron annihilation *J. Phys. F: Met. Phys.* **11** 2221–30
[30] Ashby M F 1974 A first report on sintering diagrams *Acta Metall.* **22** 275–89